The Astrophysical Journal Letters, 944:L39 (7pp), 2023 February 20 https://doi.org/10.3847/2041-8213/acb7d9

Hypervelocity Stars Track Back to the Galactic Center in Gaia DR3

Jiwei Liao[1], Cuihua Du[1], Hefan Li[2], Jun Ma[1,2], and Jianrong Shi[1,2]
[1] College of Astronomy and Space Sciences, University of Chinese Academy of Sciences, Beijing 100049, People's Republic of China; ducuihua@ucas.ac.cn
[2] Key Laboratory of Optical Astronomy, National Astronomical Observatories, Chinese Academy of Sciences, Beijing 100012, People's Republic of China
Received 2022 November 18; revised 2023 January 30; accepted 2023 February 1; published 2023 February 17

Abstract

Based on the proper motions and radial velocities from Gaia Data Release 3, we identify two hypervelocity stars (HVSs) that may originate from the Galactic center (GC). We select the candidates by first filtering for all Gaia stars with Galactocentric radial velocities $>500\,\mathrm{km\,s^{-1}}$. We also require the candidates cross the Galactic midplane only once at 80% confidence, as determined by backwards orbit integration in several models of the Galactic potential, given the uncertainties in the Gaia measurables. The final two HVS candidates are the only such stars in our sample whose backwards-integrated trajectories pass within 1 kpc of the GC, suggesting a potential GC origin. We discuss possible ejection scenarios for these HVSs, in particular, by finding that ejection via the Hills mechanism is unlikely unless the HVS trajectories were significantly altered by local or large-scale perturbations to the assumed Galactic potential, e.g., the Large Magellanic Cloud. Interestingly, one of the HVSs ejects in a direction that is curiously aligned with the clockwise stellar disk around Sgr A*, suggesting a possible connection. We also discuss that the two stars may be ejected by other mechanisms.

Unified Astronomy Thesaurus concepts: Hypervelocity stars (776); Stellar dynamics (1596); Stellar kinematics (1608); Galactic center (565); Supermassive black holes (1663)

1. Introduction

Hypervelocity stars (HVSs) move sufficiently fast so that they can escape the Galaxy. Hills (1988) first predicted the existence of HVSs with velocities of $1000\,\mathrm{km\,s^{-1}}$ and above by the dynamical interactions between stellar binaries and the supermassive black hole (SMBH) at the Galactic center (GC), Sgr A* (Reid & Brunthaler 2004; Event Horizon Telescope Collaboration et al. 2022). The GC may produce HVSs via several unique mechanisms not found elsewhere in the galaxy. These include the tidal breakup of binary stars by Sgr A* (Hills 1988); acceleration of single stars, such as Sgr A* is assumed to be one component of a binary black hole (Yu & Tremaine 2003); and interactions between Sgr A* and globular clusters (e.g., Capuzzo-Dolcetta & Fragione 2015; Fragione & Capuzzo-Dolcetta 2016). Within or beyond the GC, HVSs may also be runaways ejected by supernovae in stellar binaries (Blaauw 1961; Wang et al. 2013), strong gravitational scattering in dense stellar systems (Gvaramadze et al. 2009), or tidal stripping during the galaxy's accretion and disruption of its satellites (Abadi et al. 2009; Teyssier et al. 2009).

The first HVS was serendipitously discovered by Brown et al. (2005) in a spectroscopic survey of faint blue horizontal-branch star candidates in the Galactic halo, and it is a B-type star with a heliocentric distance ∼71 kpc and total velocity of about $709\,\mathrm{km\,s^{-1}}$, well above the escape velocity at such a distance. This discovery led to dedicated searches, and a large number of hypervelocity candidates have been reported (e.g., Edelmann et al. 2005; Hirsch et al. 2005; Brown et al. 2006, 2009, 2012, 2014, 2018; Heber et al. 2008; Kollmeier et al. 2009; Tillich et al. 2009; Li et al. 2012; Zheng et al. 2014; Huang et al. 2017; Vennes et al. 2017; Du et al. 2019; Kreuzer et al. 2020; Li et al. 2022). However, most candidates have been shown to be nonconsistent within the GC. Some candidates are thought to originate from either the stellar disk (Du et al. 2018; Hattori et al. 2019) or from the tidal debris of an accreted dwarf galaxy such as the Large Magellanic Cloud and the Sagittarius dwarf spheroidal galaxy (Erkal et al. 2019; Evans et al. 2021; Huang et al. 2021; Li et al. 2022). Recently, the Southern Stellar Stream Spectroscopic Survey (S^5) discovered the fastest HVS S5-HVS1 (Koposov et al. 2020), an A-type star with a total velocity of $1755\,\mathrm{km\,s^{-1}}$, whose backward orbit points to the GC, providing solid evidence of the GC-origin scenario. The presence of SMBH (and thus an origin in the GC) is necessary to explain the extremely high velocity of S5-HVS1.

The unconstrained velocities of HVSs allow them to travel hundreds of kiloparsecs during their lifetime, with orbits formed by underlying Galactic potentials. Thus, HVSs can not only probe the extreme dynamics and physical processes at the GC but also can be used as dynamical traces of integral properties of the galaxy. They can also be used as the tracers of the Galactic potential (Gnedin et al. 2005) and constrained solar position and velocity (Hattori et al. 2018). In addition, there have been a few studies to get the shape and orientation of the dark-matter distribution in the Milky Way (MW; e.g., Gnedin et al. 2005; Contigiani et al. 2019). However, probing the shape of the MW dark-matter halo with HVSs requires more HVSs with the GC origin (Gallo et al. 2022), and to simultaneously constrain the GC and dark halo properties by HVSs is primarily hampered by the paucity of data (e.g., Rossi et al. 2017). It is of paramount importance to search a number of HVSs with the GC origin.

The exquisite quality of data produced by Gaia allows us to renew the study of HVSs, particularly the third data release (DR3). The Gaia DR3 catalog spans 34 months of observation, provides a massive amount of new information including all-sky, precise photometric/astrometric/spectroscopic measurements (Gaia Collaboration et al. 2022), which enable us to search for new HVSs with the GC origin. In this study, we

report our search for HVSs from Gaia DR3 with full phase-space information and obtain two candidate HVSs that could be traced back to the GC. This paper is organized as follows: in Section 2, we describe the observation sample. In Section 3, we obtain two candidate HVSs originating from the GC that satisfy the selection criteria. In Section 4, we perform orbital analysis of two candidate HVSs. Finally, we give a summary and discussion in Section 5.

2. Observation Sample

Gaia DR3 provides astrophysical parameters for 470 million stars (Creevey et al. 2022) and 34 million radial velocities (Katz et al. 2022). To obtain stars with precisely measured parallax, proper motion, and radial velocity, we use the same criteria as Marchetti et al. (2022): `RUWE` (Lindegren et al. 2021a) < 1.4 `RV_ECPECTED_SIG_TO_NOISE` $\geqslant 5$, `RV_NB_TRANSITS` $\geqslant 10$ (Katz et al. 2022), and $\varpi - \varpi_{\rm ZP}$ (Lindegren et al. 2021b) > 0. If $\varpi - \varpi_{\rm ZP} < 5\sigma_{\varpi}$, we select the sample stars with the astrophysical parameter `distance_gspphot` ($d_{\rm gsp}$) provided by Gaia DR3, which is inferred by GSP-Phot Aeneas from the blue photometer (BP)/red photometer (RP) spectra, apparent G magnitude, and parallax.

We adopt the same method as Li et al. (2022) to get heliocentric distance (d) and velocity in the R.A. and decl. direction (ν_{α} and ν_{δ}) of stars with precise parallax ($\varpi - \varpi_{\rm ZP} > 5\sigma_{\varpi}$). We use the 3D posterior of Du et al. (2019) and replace the distance prior (Bailer-Jones et al. 2021) with a three-parameter generalized gamma distribution:

$$P(\theta|\chi) \propto e^{-\frac{1}{2}(\chi - m(\theta))^T C_{\chi}^{-1}(\chi - m(\theta))} \frac{1}{\Gamma\left(\frac{\beta+1}{\alpha}\right)} \frac{\alpha}{L^{\beta+1}} r^{\beta} e^{-\left(\frac{r}{L}\right)^{\alpha}}, \quad (1)$$

where $\theta = [d, \nu_{\alpha}, \nu_{\delta}]$, $\chi = [\varpi, \mu_{\alpha*}, \mu_{\delta}]$, $m = [1/d + \varpi_{\rm zp}, \nu_{\alpha}/kd, \nu_{\delta}/kd]$, $k = 4.74047$, and C_{χ} is the covariance matrix:

$$\begin{pmatrix} \sigma_{\varpi}^2 & \rho_{\varpi}^{\mu_{\alpha}*}\sigma_{\varpi}\sigma_{\mu_{\alpha}*} & \rho_{\varpi}^{\mu_{\delta}}\sigma_{\varpi}\sigma_{\mu_{\delta}} \\ \rho_{\mu_{\alpha}*}^{\varpi}\sigma_{\mu_{\alpha}*}\sigma_{\varpi} & \sigma_{\mu_{\alpha}*}^2 & \rho_{\mu_{\alpha}*}^{\mu_{\delta}}\sigma_{\mu_{\alpha}*}\sigma_{\mu_{\delta}} \\ \rho_{\mu_{\delta}}^{\varpi}\sigma_{\mu_{\delta}}\sigma_{\varpi} & \rho_{\mu_{\delta}}^{\mu_{\alpha}*}\sigma_{\mu_{\delta}}\sigma_{\mu_{\alpha}*} & \sigma_{\mu_{\delta}}^2 \end{pmatrix}, \quad (2)$$

where ρ_i^j denotes the correlation coefficient between i and j, σ_k denotes the standard deviation of k, and $i = \varpi, \mu_{\alpha}^*, \mu_{\delta}$.

We use the Markov Chain Monte Carlo sampler, emcee (Foreman-Mackey et al. 2013), to draw samples from the posterior probability. In this study, we generate 5000 Monte Carlo (MC) realizations for each star and use the median value to describe the results. The lower and upper uncertainties are the 16th and 84th percentiles of the probability distribution function. At large parallax uncertainties, the photogeometric distances will generally be more precise than geometric ones (Bailer-Jones et al. 2021). In this study, heliocentric distance of stars without precise parallax ($\varpi - \varpi_{\rm ZP} < 5\sigma_{\varpi}$) is $d_{\rm gsp}$. We assume that proper motions and $d_{\rm gsp}$ are not correlated, and the distance error ($\sigma_{d_{\rm gsp}}$) is the average of $d_{\rm gsp} -$ `distance_gspphot_lower` and `distance_gspphot_upper` $- d_{\rm gsp}$. We use the same sampler method to draw 5000 MC realizations of each star from a multivariate Gaussian distribution, with mean vector $m = [\nu_{\alpha}/kd_{\rm gsp}, \nu_{\delta}/kd_{\rm gsp}, d_{\rm gsp}]$ and covariance matrix

$$\begin{pmatrix} \sigma_{\mu_{\alpha}*}^2 & \rho_{\mu_{\alpha}*}^{\mu_{\delta}}\sigma_{\mu_{\alpha}*}\sigma_{\mu_{\delta}} & 0 \\ \rho_{\mu_{\delta}}^{\mu_{\alpha}*}\sigma_{\mu_{\delta}}\sigma_{\mu_{\alpha}*} & \sigma_{\mu_{\delta}}^2 & 0 \\ 0 & 0 & \sigma_{d_{gsp}}^2 \end{pmatrix}. \quad (3)$$

To derive the 3D velocities (U, V, and W; Johnson & Soderblom 1987) and the position of each star in the right-handed Cartesian Galactocentric coordinate system (Jurić et al. 2008), we adopt the position of the Sun to the GC, $(x_{\odot}, y_{\odot}, z_{\odot}) = (8.122, 0, 0.0208)$ kpc (GRAVITY Collaboration et al. 2018; Bennett & Bovy 2019) and solar velocity of $(U_{\odot}, V_{\odot}, W_{\odot}) = (11.1, 245, 7.25)$ km s^{-1} (Schönrich et al. 20102010; McMillan 2017).

3. Searching for Candidate HVSs

If HVSs are ejected from the GC by the Hills mechanism, the ejection velocity is approximately equal to the Galactocentric radial velocities ($\nu_{\rm ej} \approx \nu_{\rm r_{GC}}$) that can approach as high as 1000 km s^{-1} or more. After the GC ejects an HVS, the gravitational potential of the MW decelerates the outbound HVS, decreasing $\nu_{\rm r_{GC}}$. To obtain reliable HVSs, we select stars with $\nu_{\rm r_{GC}}$ greater than half of the ejection velocity ($\nu_{\rm r_{GC}} > 500$ km s^{-1}). For the stars with $\nu_{\rm r_{GC}} > 500$ km s^{-1}, we use `galpy` (Bovy 2015) to integrate the backward orbit over a total time of 1 Gyr with a time step of 0.1 Myr in four different potential models. The four potential models are Gala, Bo15, Mc17, and Ca20 (Bovy 2015; McMillan 2017; Price-Whelan 2017; Cautun et al. 2020). It is difficult to judge the origins of HVSs with backward orbits that cross the Galactic midplane more than once. Thus, we select the stars that cross over the Galactic midplane ($Z_{\rm GC} = 0$ kpc plane) only once and whose backwards-integrated trajectories pass within 1 kpc of the GC($r_{\rm closest} < 1$ kpc) as candidate HVSs originating from the GC.

Figure 1 shows the probability ($P_{\rm cross}$) of HVSs with $\nu_{\rm r_{GC}} > 500$ km s^{-1} that cross over the Galactic midplane ($Z_{\rm GC} = 0$ kpc plane) only once under the four potential models. The vertical dashed line denotes the cut $P_{\rm cross} > 0.8$, used to determine HVSs whether cross over the Galactic midplane only once. Figure 2 shows the position and velocity vector of HVSs with $\nu_{\rm r_{GC}} > 500$ km s^{-1} and $P_{\rm cross} > 0.8$ that have backwards-integrated orbits passing close to the GC. Two of the HVSs, Gaia DR3 6016819861087891456 and Gaia DR3 4094201527955913856, pass especially close to the GC ($r_{\rm closest} < 1$ kpc). We select these two stars as the most likely of our HVS candidates to have originated in the GC. The velocity directions of these two stars change little between their present-day and perigalactic positions; due to their high speeds, the Galactic potential accelerates these HVSs little during this traverse. For each of these HVSs and for each different Galactic potential model, Table 1 lists the perigalactic distance and velocity ($r_{\rm closest}$ and $\nu_{\rm closest}$, respectively), as well as the time $t_{\rm closest}$ taken for the stars to traverse from their perigalactic to present-day positions.

4. Orbit Analysis

We now more thoroughly examine the orbits, including associated uncertainties, of the two HVSs selected in Section 3 as most likely to have originated in the GC. Since the Galactic field is a classically collisionless system, particularly at the high

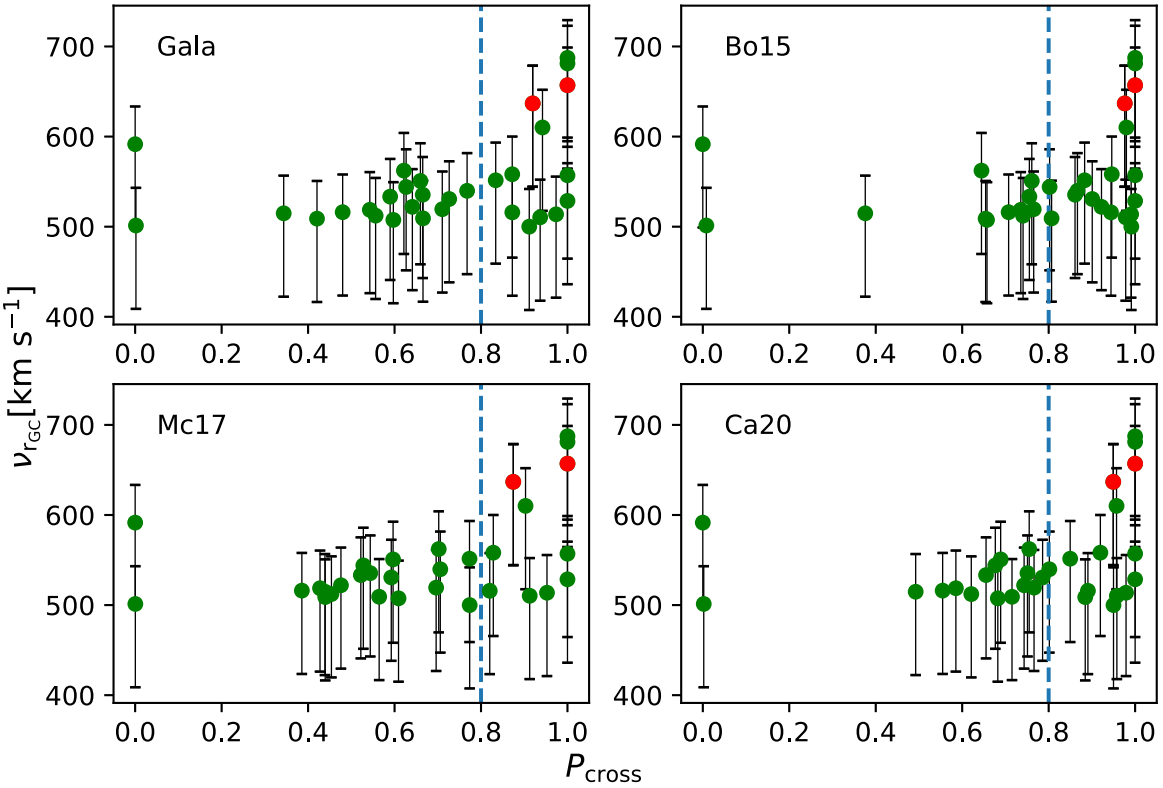

Figure 1. Distribution of the Galactocentric radial velocities ($\nu_{\rm rGC}$) vs. the probability ($P_{\rm cross}$) that HVSs cross over the Galactic midplane ($Z_{\rm GC} = 0$ kpc plane) only once under the four potential models. Green points mark HVSs with $\nu_{\rm rGC} > 500$ km s^{-1}, and red points mark the two HVSs tracking back to the GC. The vertical dashed line denotes the cut $P_{\rm cross} > 0.8$, used to search for HVSs which cross over the Galactic midplane only once.

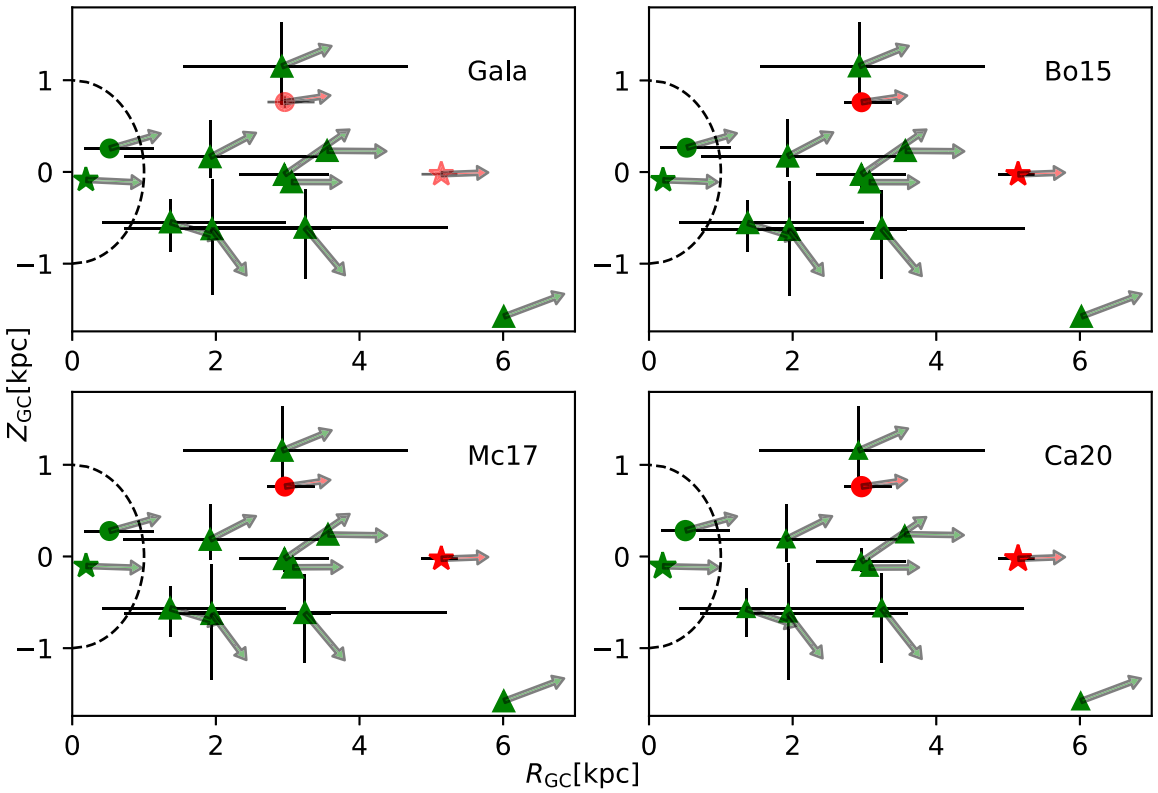

Figure 2. Distribution in Galactocentric cylindrical coordinates ($R_{\rm GC}$, $Z_{\rm GC}$) of the sample stars with $\nu_{\rm rGC} > 500$ km s^{-1} and $P_{\rm cross} > 0.8$ under the four potentials models. Green symbols mark the closest position of the sample stars to the GC. Red filled circle and red star mark the current position of Gaia DR3 6016819861087891456 and Gaia DR3 4094201527955913856, respectively. Arrows point in the direction of the total velocity vector, and their length is proportional to the total velocity. The dashed line forming a semicircle denotes the cut $r_{\rm closest} < 1$ kpc, used to search for candidate HVSs originating from the GC.

Table 1
The Relevant Parameters of the Candidate HVSs Tracking Back to the GC

Gaia DR3 ID …	$v_{r_{GC}}$ (km s^{-1})	Potentials …	P_{cross} …	$r_{closest}$ (pc)	$v_{closest}$ (km s^{-1})	$t_{closest}$ (Myr)
6016819861087891456	637^{+42}_{-93}	Gala	0.9196	583^{+588}_{-280}	742^{+32}_{-94}	4.4^{+1}_{-0}
6016819861087891456	637^{+42}_{-93}	Bo15	0.976	589^{+586}_{-280}	723^{+45}_{-80}	4.4^{+1}_{-0}
6016819861087891456	637^{+42}_{-93}	Mc17	0.8746	590^{+589}_{-268}	733^{+42}_{-83}	4.4^{+1}_{-0}
6016819861087891456	637^{+42}_{-93}	Ca20	0.9494	586^{+577}_{-260}	745^{+37}_{-86}	4.4^{+1}_{-0}
4094201527955913856	$657^{+0.1}_{-0.2}$	Gala	1	209^{+72}_{-79}	795^{+11}_{-5}	7.1^{+3}_{-4}
4094201527955913856	$657^{+0.1}_{-0.3}$	Bo15	1	214^{+73}_{-76}	$770^{+0.5}_{-0.1}$	7.1^{+3}_{-4}
4094201527955913856	$657^{+0.1}_{-0.3}$	Mc17	1	218^{+70}_{-72}	$783^{+0.2}_{-0.4}$	7.1^{+3}_{-4}
4094201527955913856	$657^{+0.1}_{-0.3}$	Ca20	1	218^{+68}_{-74}	$796^{+0.4}_{-0.8}$	7.1^{+3}_{-4}

speeds typical of HVSs, we neglect the perturbative influence of other bodies on these orbits and consider only the impact of the global Galactic potential. Hyperbolic trajectories this deep in the Galactic potential are highly nonlinear and feature relatively sharp turning points at the perigalacticon. As shown in Figure 3, the thin gray lines show 1000 orbits drawn at random from the uncertainties in the positions and velocities of each of the two HVSs, showing the uncertainty in the orbits. Their orbits are highly nonlinear and take a turn at the perigalacticon. The closest position from the GC is located at the orbit turning point in Figure 4. If the two stars originated from the GC, we may consider the backward orbital turning point as the ejection point so that the position, velocity, and backward time at the orbit turning point are the ejection position, ejection velocity, and flight time.

The flight direction of HVSs originating from the GC should be approximately aligned (Lu et al. 2010; Zhang et al. 2010) with the orbital plane of the original binary around the SMBH and the orbital plane of the secondary star captured by the SMBH after the binary disruption (unless the secondary was swallowed by the black hole and/or produced a tidal disruption event; Koposov et al. 2020). The orbit orientations are consistent with the flight direction. Orbit orientations of Gaia DR3 6016819861087891456 cross the clockwise stellar disk in Figure 5, meaning that it flies within the orbital plane of young stars around the GC. This is potentially very interesting because it may mean that the binary responsible for Gaia DR3 6016819861087891456 has the same origin as the clockwise stellar disk.

The probability of an ejection by the Hills mechanism (Bromley et al. 2006) is as follows:

$$P_{ej} \approx \begin{cases} 1 - D_{min}/175, & \text{if } 0 \leqslant D_{min} \leqslant 175 \\ 0, & \text{otherwise,} \end{cases} \quad (4)$$

where

$$D_{min} = \frac{R_{min}}{a_{bin}} \left[\frac{2M_{bh}}{10^6(m_1 + m_2)} \right]^{-1/3}, \quad (5)$$

where R_{min} is the closest distance of the binary star to the black hole, a_{bin} is the semimajor axis of the binary, M_{bh}, $m1$, and $m2$ are the masses of the black hole and the binary, respectively. However, R_{min} (i.e., $r_{closest}$ in our study) $\gg a_{bin}$ indicates $D_{min} > 175$ and $P_{ej} = 0$. This does not mean that the two HVSs are not ejected by the Hills mechanism because the orbital uncertainty could increase D_{min} to more than 175. The small error in $r_{closest}$ suggests that statistical error is not the main reason. Additional gravitational influences may cause changes in the orbits of stars after they are ejected, such as deflection of the HVSs by the pull of the Large Magellanic Cloud on the MW (Kenyon et al. 2018; Boubert et al. 2020).

5. Summary and Discussion

In this study, based on the high-quality positions, proper motions, and parallaxes of Gaia DR3, we search for HVSs originating from the GC. We perform backward orbital integration for the stars with $v_{r_{GC}} > 500\,\mathrm{km\,s^{-1}}$, obtaining the two HVSs that cross the Galactic midplane ($Z_{GC} = 0$ kpc plane) only once at 80% confidence and cross the vicinity of the GC (within 1 kpc of the GC). By analyzing the orbits of the two stars, we find that it is impossible for the stars to be ejected via the Hills mechanism unless they are subject to additional gravitational influences, such as the Large Magellanic Cloud. The direction of the Gaia DR3 6016819861087891456 ejection is curiously aligned with stars of the clockwise stellar disk around Sgr A* and thus may be linked to its formation. Equation (4) shows that the Hills mechanism requires the binary to be close enough to Sgr A*. If we find an HVS that satisfies our election criteria and Equation (4), we will predict the position of Sgr *A by its backward orbital turning point.

Compared with the results provided by Marchetti et al. (2022), they do not derive that the two stars may originate from the GC due to the different selection criteria. They use the intersection between the backward orbit and the Galactic midplane ($Z_{GC} = 0$ kpc plane) is less than 1 kpc. But the ejection positions of the HVSs' origin from the GC do not necessarily lie on the Galactic midplane, and the location where the backward orbit is closest to the GC may be the ejection position. So we adopted the closest distance from the GC to be less than 1 kpc.

We could not exclude the possibility that the two stars may be ejected by other mechanisms, passing through the GC from an ejection location elsewhere. For example, the HVSs generated by encounters of stellar binaries with an intermediate-mass black hole in the core of a star cluster (Fragione & Gualandris 2019) or by three-body binary formation may dominate HVS ejection from globular clusters (Weatherford et al. 2022). The two stars may not have been ejected by a supernova explosion (SNE). It is because this mechanism is mainly to account for the existence of OB runaway stars above the Galactic plane (Blaauw 1961). And HVSs with velocities above 1000 km s^{-1} can be ejected in SNE, with progenitors of either white dwarf (WD) binaries (e.g., Shen et al. 2018) or binaries comprising a WD plus a hot subdwarf helium star

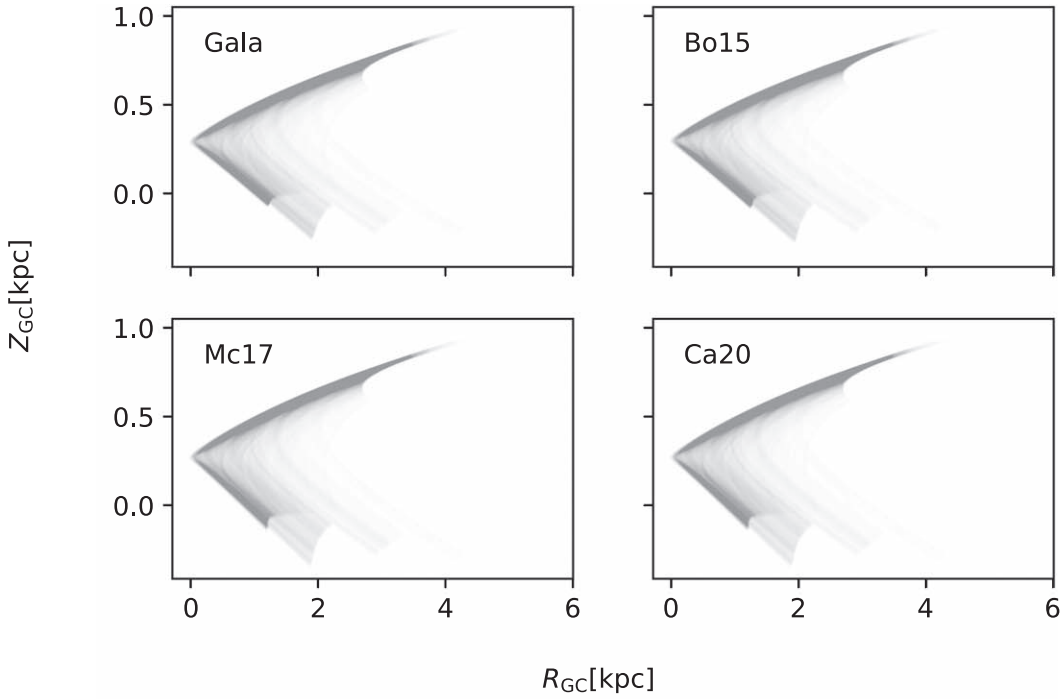

(a)

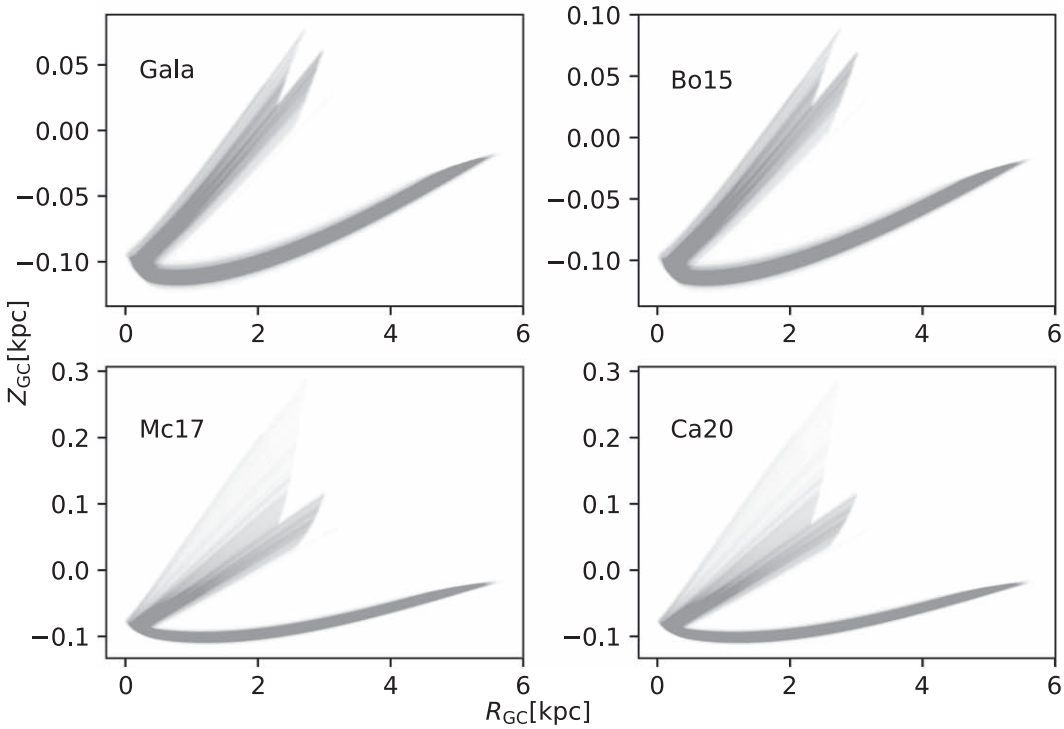

(b)

Figure 3. Panel (a) and panel (b) are 1000 orbits of Gaia DR3 6016819861087891456 and Gaia DR3 4094201527955913856 in Galactocentric cylindrical coordinates (R_{GC}, Z_{GC}) under the four potential models, respectively. These orbits drawn at random from the uncertainties in the positions and velocities of each of the two HVSs show the uncertainty in the orbits. Their orbits are highly nonlinear and take a turn at the perigalacticon.

(e.g., Bauer et al. 2019; Neunteufel 2020). According to `teff_gspphot` and `logg_gspphot` provided by Gaia DR3, Gaia DR3 4094201527955913856, with an effective temperature of 8399 K and surface gravity $\log g = 2.85^{+0.01}_{-0.02}$, is an A-type subgiant; Gaia DR3 6016819861087891456, with an effective temperature of 6109 K and surface gravity

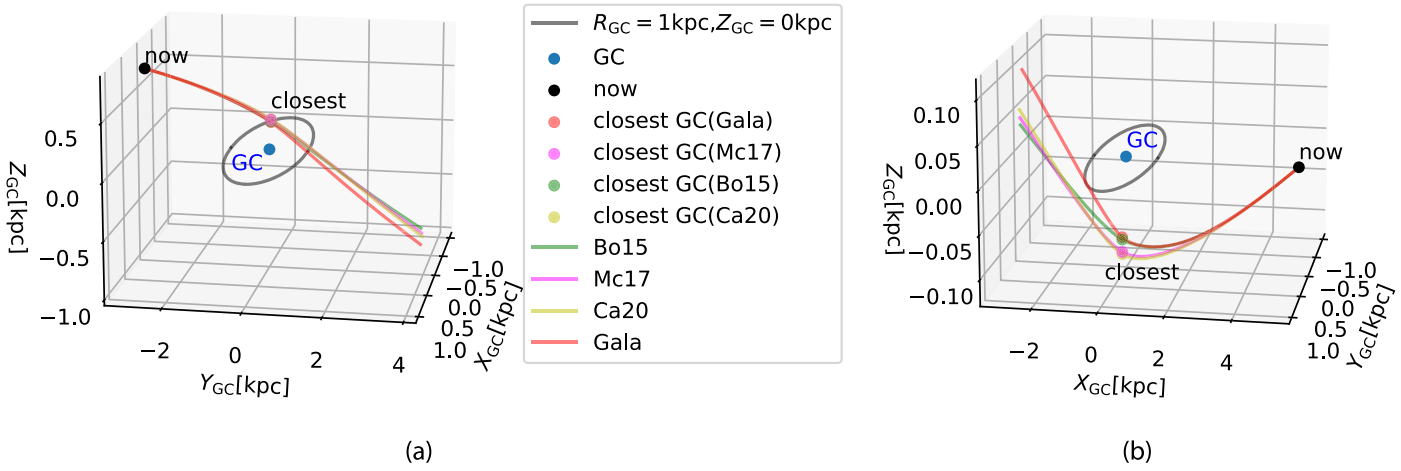

Figure 4. Panel (a) and panel (b) are the 3D backward orbits of Gaia DR3 6016819861087891456 and Gaia DR3 4094201527955913856 under four potential models, respectively. The orbits under each potential model overlap each other, and the points on the orbit closest to the GC are the same. The points on the orbit closest from the GC is the orbit turning points.

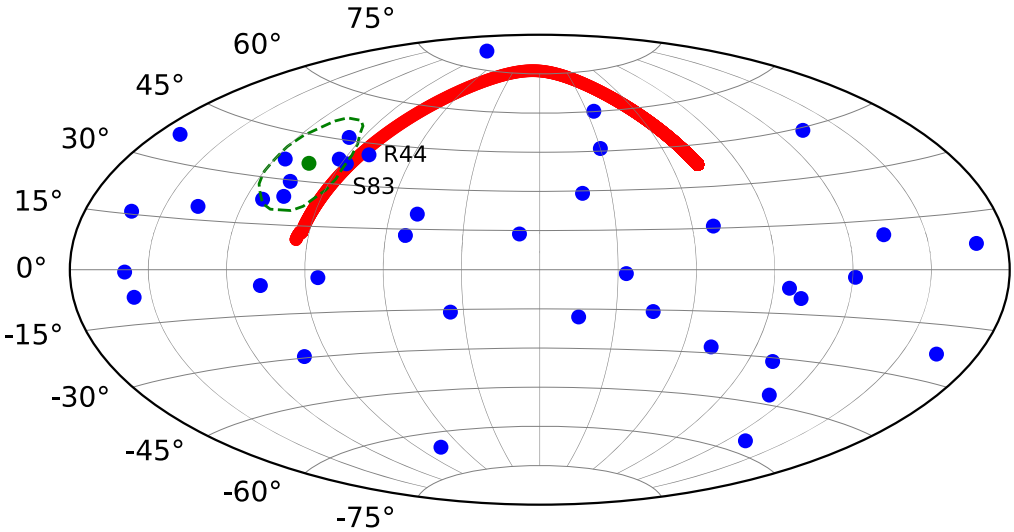

Figure 5. The coordinate system of the figure is the positional angle of ascending node of the orbit vs. inclination of the orbit with respect to the line of sight. Filled blue circles identify orientation of orbital planes of S-stars around the GC from Gillessen et al. (2017), while the red curve shows a set of possible orientations of orbital planes consistent with Gaia DR3 6016819861087891456. The red curve also identifies the potential orbital plane of the secondary star of Gaia DR3 6016819861087891456 binary if it still orbits the SMBH and if it was ejected by Hills mechanism. The stars S83 and R44 are members of the clockwise stellar disk (Bartko et al. 2009; Yelda et al. 2014) at (104°, 126°) marked by the filled green circle and the dashed line, indicating a disk thickness of 16°.

$\log g = 1.98^{+0.02}_{-0.07}$, is an F-type giant. It is known that S5-HVS1 is also an A-type star, but so far no F-type HVSs originated from the GC have been found. Regretfully, we did not find any observation of Gaia DR3 6016819861087891456 in other large-survey data, and the Gaia DR3 4094201527955913856 image was given only in SDSS DR17 (York et al. 2000; Yanny et al. 2009; Abdurro'uf et al. 2022). In the near future, we look forward to the accurate observation and spectrum identification for our two candidate HVSs as they can provide more accurate trajectory calculations. We also expect that future surveys will provide a rich source of more candidate HVSs from the GC.

We thank especially the referee for insightful comments and suggestions, which have improved the paper significantly. This work was supported by the National Natural Sciences Foundation of China (NSFC Nos. 11973042, 11973052 and 11873053). It was also supported by the Fundamental Research Funds for the Central Universities and the National Key R&D Program of China No. 2019YFA0405501. This work has made use of data from the European Space Agency (ESA) mission Gaia (https://www.cosmos.esa.int/gaia), processed by the Gaia Data Processing and Analysis Consortium (DPAC, https://www.cosmos.esa.int/web/gaia/dpac/consortium). Funding for the DPAC has been provided by national institutions, in particular the institutions participating in the Gaia Multilateral Agreement.

ORCID iDs

Jiwei Liao https://orcid.org/0000-0001-6762-5599
Cuihua Du https://orcid.org/0000-0002-3954-617X
Hefan Li https://orcid.org/0000-0002-9497-8127
Jun Ma https://orcid.org/0000-0001-6329-6644

Jianrong Shi https://orcid.org/0000-0002-0349-7839

References

Abadi, M. G., Navarro, J. F., & Steinmetz, M. 2009, ApJL, 691, L63
Abdurro'uf, Accetta, K., Aerts, C., et al. 2022, ApJS, 259, 35
Bailer-Jones, C. A. L., Rybizki, J., Fouesneau, M., et al. 2021, AJ, 161, 147
Bartko, H., Martins, F., Fritz, T. K., et al. 2009, ApJ, 697, 1741
Bauer, E. B., White, C. J., & Bildsten, L. 2019, ApJ, 887, 68
Bennett, M., & Bovy, J. 2019, MNRAS, 482, 1417
Blaauw, A. 1961, BAN, 15, 265
Boubert, D., Erkal, D., & Gualandris, A. 2020, MNRAS, 497, 2930
Bovy, J. 2015, ApJS, 216, 29
Bromley, B. C., Kenyon, S. J., Geller, M. J., et al. 2006, ApJ, 653, 1194
Brown, W. R., Geller, M. J., & Kenyon, S. J. 2009, ApJ, 690, 1639
Brown, W. R., Geller, M. J., & Kenyon, S. J. 2012, ApJ, 751, 55
Brown, W. R., Geller, M. J., & Kenyon, S. J. 2014, ApJ, 787, 89
Brown, W. R., Geller, M. J., Kenyon, S. J., & Kurtz, M. J. 2005, ApJL, 622, L33
Brown, W. R., Geller, M. J., Kenyon, S. J., & Kurtz, M. J. 2006, ApJ, 647, 303
Brown, W. R., Lattanzi, M. G., Kenyon, S. J., & Geller, M. J. 2018, ApJ, 866, 39
Capuzzo-Dolcetta, R., & Fragione, G. 2015, MNRAS, 454, 2677
Cautun, M., Benítez-Llambay, A., Deason, A. J., et al. 2020, MNRAS, 494, 4291
Contigiani, O., Rossi, E. M., & Marchetti, T. 2019, MNRAS, 487, 4025
Creevey, O. L., Sordo, R., Pailler, F., et al. 2022, arXiv:2206.05864
Du, C., Li, H., Newberg, H. J., et al. 2018, ApJL, 869, L31
Du, C., Li, H., Yan, Y., et al. 2019, ApJS, 244, 4
Edelmann, H., Napiwotzki, R., Heber, U., et al. 2005, ApJL, 634, L181
Erkal, D., Boubert, D., Gualandris, A., et al. 2019, MNRAS, 483, 2007
Evans, F. A., Marchetti, T., Rossi, E. M., et al. 2021, MNRAS, 507, 4997
Event Horizon Telescope Collaboration, Akiyama, K., Alberdi, A., et al. 2022, ApJL, 930, L12
Foreman-Mackey, D., Hogg, D. W., Lang, D., & Goodman, J. 2013, PASP, 125, 306
Fragione, G., & Capuzzo-Dolcetta, R. 2016, MNRAS, 458, 2596
Fragione, G., & Gualandris, A. 2019, MNRAS, 489, 4543
Gaia Collaboration, Vallenari, A., & Brown, A. G. A. 2022, arXiv:2208.00211
Gallo, A., Ostorero, L., Chakrabarty, S. S., et al. 2022, A&A, 663, A72
Gillessen, S., Plewa, P. M., Eisenhauer, F., et al. 2017, ApJ, 837, 30
Gnedin, O. Y., Gould, A., Miralda-Escudé, J., & Zentner, A. R. 2005, ApJ, 634, 344
GRAVITY Collaboration, Abuter, R., Amorim, A., et al. 2018, A&A, 615, L15
Gvaramadze, V. V., Gualandris, A., & Zwart, S. P. 2009, MNRAS, 396, 570
Hattori, K., Valluri, M., & Castro, N. 2018, ApJ, 869, 33
Hattori, K., Valluri, M., Castro, N., et al. 2019, ApJ, 873, 116
Heber, U., Edelmann, H., Napiwotzki, R., et al. 2008, A&A, 483, L21
Hills, J. G. 1988, Natur, 331, 687
Hirsch, H. A., Heber, U., O'Toole, S. J., & Bresolin, F. 2005, A&A, 444, L61
Huang, Y., Li, Q., Zhang, H., et al. 2021, ApJL, 907, L42
Huang, Y., Liu, X.-W., Zhang, H.-W., et al. 2017, ApJL, 847, L9
Johnson, D. R. H., & Soderblom, D. R. 1987, AJ, 93, 864
Jurić, M., Ivezić, Ž., Brooks, A., et al. 2008, ApJ, 673, 864
Katz, D., Sartoretti, P., Guerrier, A., et al. 2022, arXiv:2206.05902
Kenyon, S. J., Bromley, B. C., Brown, W. R., & Geller, M. J. 2018, ApJ, 864, 130
Kollmeier, J. A., Gould, A., Knapp, G., & Beers, T. C. 2009, ApJ, 697, 1543
Koposov, S. E., Boubert, D., Li, T. S., et al. 2020, MNRAS, 491, 2465
Koposov, S., Irrgang, A., Heber, U., et al. 2020, A&A, 637, A53
Li, H., Du, C., Ma, J., et al. 2022, ApJL, 933, L13
Li, Q.-Z., Huang, Y., Dong, X.-B., et al. 2022, arXiv:2207.04406
Li, Y., Luo, A., Zhao, G., et al. 2012, ApJL, 744, L24
Lindegren, L., Bastian, U., Biermann, M., et al. 2021a, A&A, 649, A4
Lindegren, L., Klioner, S. A., Hernández, J., et al. 2021b, A&A, 649, A2
Lu, Y., Zhang, F., & Yu, Q. 2010, ApJ, 709, 1356
Marchetti, T., Evans, F. A., & Rossi, E. M. 2022, MNRAS, 515, 767
McMillan, P. J. 2017, MNRAS, 465, 76
Neunteufel, P. 2020, A&A, 641, A52
Price-Whelan, A. M. 2017, JOSS, 2, 388
Reid, M. J., & Brunthaler, A. 2004, ApJ, 616, 872
Rossi, E.M., Marchetti, T., Cacciato, M., et al. 2017, MNRAS, 467, 1844
Schönrich, R., Binney, J., & Dehnen, W. 2010, MNRAS, 403, 1829
Shen, K. J., Boubert, D., Gänsicke, B. T., et al. 2018, ApJ, 865, 15
Teyssier, M., Johnston, K. V., & Shara, M. M. 2009, ApJL, 707, L22
Tillich, A., Przybilla, N., Scholz, R.-D., & Heber, U. 2009, A&A, 507, L37
Vennes, S., Nemeth, P., Kawka, A., et al. 2017, Sci, 357, 680
Wang, B., Justham, S., & Han, Z. 2013, A&A, 559, A94
Weatherford, N. C., Kıroğlu, F., Fragione, G., et al. 2022, arXiv:2211.16523
Yanny, B., Rockosi, C., Newberg, H. J., et al. 2009, AJ, 137, 4377
Yelda, S., Ghez, A. M., Lu, J. R., et al. 2014, ApJ, 783, 131
York, D. G., Adelman, J., Anderson, J. E., Jr., et al. 2000, AJ, 120, 1579
Yu, Q., & Tremaine, S. 2003, ApJ, 599, 1129
Zhang, F., Lu, Y., & Yu, Q. 2010, ApJ, 722, 1744
Zheng, Z., Carlin, J. L., Beers, T. C., et al. 2014, ApJL, 785, L23